Journal of
Materials Chemistry A

Materials for energy and sustainability

Accepted Manuscript

This article can be cited before page numbers have been issued, to do this please use: J. M. Bermúdez-García, S. Yañez, Á. Ferradanes Martínez, A. L. Llamas-Saiz, M. Sánchez-Andújar, S. Castro-Garcia, M. A. Señarís-Rodríguez and J. Mira Pérez, *J. Mater. Chem. A*, 2026, DOI: 10.1039/D6TA00623J.

ROYAL SOCIETY OF CHEMISTRY

rsc.li/materials-a

View Article Online
DOI: 10.1039/D6TA00623J

ARTICLE

Giant electrocaloric response in thiourea under low electric field in the cryogenic region

Received 00th January 20xx,
Accepted 00th January 20xx

DOI: 10.1039/x0xx00000x

Juan Manuel Bermúdez-García,[a‡*] Susana Yáñez-Vilar,[b‡] Angel Ferradanes -Martínez,[a] Antonio Luis Llamas-Saiz,[c] Manuel Sánchez-Andújar,[a] Socorro Castro-García,[a] María Antonia Señarís-Rodríguez,[a] and Jorge Mira.[b**]

In this work, almost 70 years after thiourea ferroelectricity was discovered, we report hitherto undiscovered electrocaloric properties in this compound. Remarkably, we report a giant electrocaloric strength ($\Delta S/\Delta E$ = 1.13 J cm kg^{-1} kV^{-1}) and a large electrocaloric tunability (dT_t/dE = 0.7 K cm kV^{-1}) that range within the values obtained for the best bulk electrocaloric materials reported up to date and, moreover, requiring an outstanding low electric field. Furthermore, we identify that the electrocaloric effects can be further enhanced through the application of external pressure, turning this material into a new example of the emerging family of multicaloric materials. We relate such giant electrocaloric parameters to the large dielectric dipole, low molecular weight and weak chemical interactions, especially H-bonds, between the molecules that conform thiourea. Interestingly, these electrocaloric effects take place near 170 K, which could be useful for electrocaloric cooling supporting liquid nitrogen cryogenic systems.

1. Introduction

In 1828, Friedich Wöhler gave birth to the modern organic chemistry with the synthesis of urea –CH_4N_2O–, the first organic compound directly obtained from an inorganic compound.[1] A few years later, Marceli Nencki obtained in his laboratory the analogue sulfur compound, thiourea –CH_4N_2S–,[2] which was one of the earliest organic crystal structures to be studied[3] and to show ferroelectric properties[4]. Intensive studies on its unique ferroelectric behaviour have been performed since then.[5–11]

This compound exhibits multiple dielectric transitions associated to different solid-solid phase transitions. From the structural point of view, thiourea crystals present five different polymorphs as a function of temperature. The low temperature phase I (T < 168 K) shows orthorhombic symmetry with non-centrosymmetric space group ($P2_1ma$), while the high temperature phase V (T > 202 K) exhibits orthorhombic symmetry with centrosymmetric space group ($Pnma$)[5]. The intermediate phases II to IV are modulated phases traditionally described as the result of sinusoidal modulations of the displacement of the atoms.[8] The original studies from Goldsmith and White demonstrated that phases I and III are ferroelectric, II and IV are antiferroelectric, and V is paraelectric.[5] Meanwhile, later studies revealed that the transition temperatures of the different structures can be shifted as a function of the electric field.[6,11] Moreover, the are some –even if scarce– studies on thiourea thermal properties[6,12] showing that the largest thermal changes occur for the first transition between phases I and II, with values of 6.6 cal/mol (380 J kg^{-1}). On the basis of the reported ferroelectric and thermal properties, we anticipate that thiourea can present interesting electrocaloric effects, which have not been explored up to date.

Electrocaloric materials are compounds that exhibit large thermal changes (isothermal entropy changes or adiabatic temperature changes) under the application and removal of an external electric field, generally associated to first-order ferroelectric transitions.[13] This family of functional materials is very interesting for heating and cooling applications and can be the basis for more efficient and eco-friendly refrigeration technologies.[14,15] Particularly, cryogenic refrigeration is becoming a growing challenge in our society. Emerging technologies such as wind generators using superconducting materials,[16] to cryogenic sensors and instruments in the re-activated space race need temperatures in the range of 150 K and below.[17] Technologies based on cryogenic liquids (especially liquid nitrogen) are a relatively easy and economic method to reach such temperatures. However, these technologies can produce leaks and fluid losses and –in some cases- they can present carbon emissions similar to diesel-driven vapour compression systems.[18] For those reasons, new cryogenic technologies, such as cryocoolers, are being explored to use in replacement and/or in combination with cryogenic fluids. In that regard, recent reports highlight that one of the

[a]. CICA–Centro Interdisciplinar de Química e Bioloxía and Departamento de Química, Facultade de Ciencias, Universidade da Coruña, 15071 A Coruña, Spain. *j.bermudez@udc.es
[b]. Departamento de Física Aplicada and Instituto de Materiais (iMATUS), Universidade de Santiago de Compostela, 15782, Santiago de Compostela, Spain. **jorge.mira@usc.es
[c]. Research Infrastructures Area X-ray Unit, Universidade de Santiago de Compostela, 15782 Santiago de Compostela, Spain.
† These authors have equally contributed to this work.
Supplementary Information available: [details of any supplementary information available should be included here]. See DOI: 10.1039/x0xx00000x.

View Article Online
DOI: 10.1039/D6TA00623J

potential applications for electrocaloric materials yet to be explored is cryogenic refrigeration, where examples of electrocaloric materials is very limited since most of them operate between 250 and 500 K.[19–22]

From the technological point of view, an important challenge concerns the operating electric field required to induce the thermal changes. Meanwhile reported electrocalorics in *bulk* can show larger energy density, they also require very large electric fields to exhibit sufficient caloric effects. For that reason, in the last year most efforts have been devoted to develop thin-films and multilayer electrocalorics, where the required electric field is dramatically reduced, but the active mass is limited by the thickness and number of the deposited layers.[19–22]

Inspired by previous results, where we identified new stimuli-induced functional properties and caloric effects in both classic compounds –such as inorganic perovskites and intermetallic compounds–[23,24] and emerging materials –such as hybrid perovskites and metal-organic frameworks or MOFs–[25,26], we have intuited that the classic ferroelectric compound thiourea could present hitherto undiscovered electrocaloric effects in *bulk* state, with a large response under electric field in the cryogenic temperature range. In that case, it would be useful for potential cryogenic refrigeration.

Surprisingly, and as we will show, this material exhibits a electrocaloric effect very similar to that found in the best *bulk* electrocaloric materials, and even larger in some cases.[19–22] Moreover, thiourea exhibits a giant electrocaloric strength (dS/dE) and a large tunability (dT_t/dE) due to a remarkably large sensibility towards electric field. In addition, we deepen into the relationship between the electrocaloric properties and the crystal structure of this compound in order to identify the key aspects that make this material very sensible to the electric field, a most interesting aspect for the design of future electrocaloric materials.

2. Results and discussion

2.1. Variable-temperature differential scanning calorimetry and dielectric studies.

We have performed variable-temperature differential scanning calorimetry (VT-DSC) to evaluate the latent heat related to the phase transitions of thiourea. To the best of our knowledge most DSC studies on thiourea have been focused on evaluating the specific heat capacity upon heating and/or monitor the melting and thermal decomposition of thiourea coupled with thermogravimetric analysis (TGA).[12,27–30] These previous DSC studies under heating revealed that the more energetic thermal transition is observed at ~170 K, while the rest of the transitions show a significantly much lower energy and/or are difficult to observe by calorimetry.[6,30] For that reason, we focus our studies in the narrow vicinity of this particular transition. In that regard, Figure 1 shows the more energetic phase transition, corresponding to the transition I-II. This structural change occurs at a transition temperature of T_h ~ 169.6 K on heating and T_c ~ 168.6 K on cooling, being the first DSC studies –to our knowledge– that evaluate the reversibility of the phase transition upon heating and cooling.

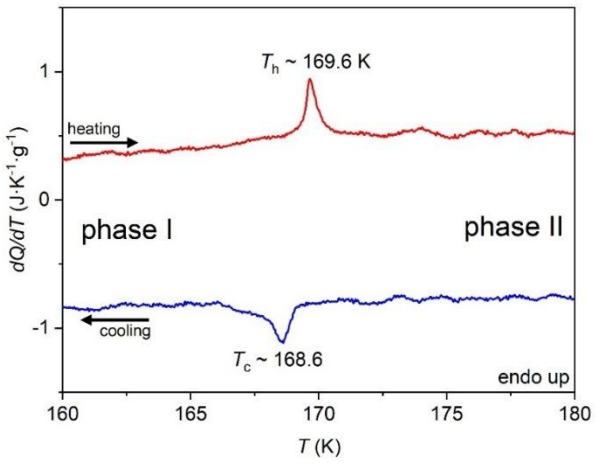

Figure 1. Heat flow dQ/dT on cooling (blue) and heating (red) measured from 160 to 180 K at a rate of 1 K min^{-1}.

Remarkable, our results show that the thermal hysteresis of this transition is very low with values of (T_h-T_c) ~ 1.0 K, which is desired in caloric materials for reducing thermal losses associated with large thermal hysteresis.[31] Furthermore, the latent heat values of this transition is as large as ΔH ~ 340 J kg^{-1}, which is in agreement with the literature,[6] and more importantly is similar to those values observed for electrocaloric ceramics.[20]

In addition, we have also studied the temperature dependence of the real part of the relative permittivity along the polar *a*-axis as shown in Figure 2. Here we can observe anomalies of the real part of the relative permittivity related to the structural phase transitions between the different polymorphs (I, II, III, IV and V), in full agreement with literature data.[5]

The first dielectric transition from the ferroelectric (FE) phase I to the antiferroelectric (AFE) phase II starts at 168 K. The second transition between II (AFE) and III (FE) starts at 175 K.

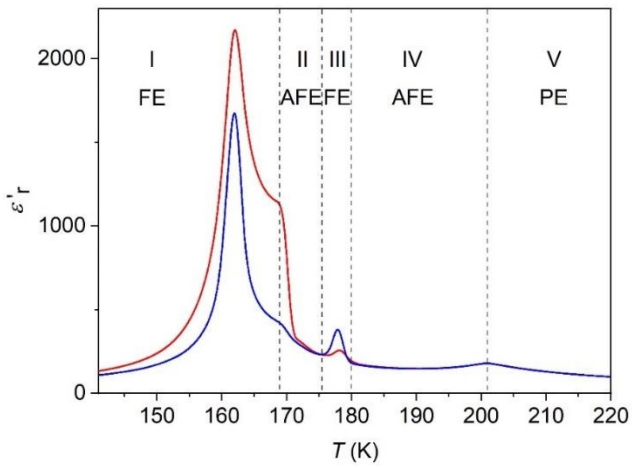

View Article Online
DOI: 10.1039/D6TA00623J

Figure 2. Dielectric permittivity along the polar axis (ε'_r) versus temperature (T) on cooling (blue) and heating (red) at ν = 1 MHz. Note: Regions I to V have been assigned according to references [5,6,8].

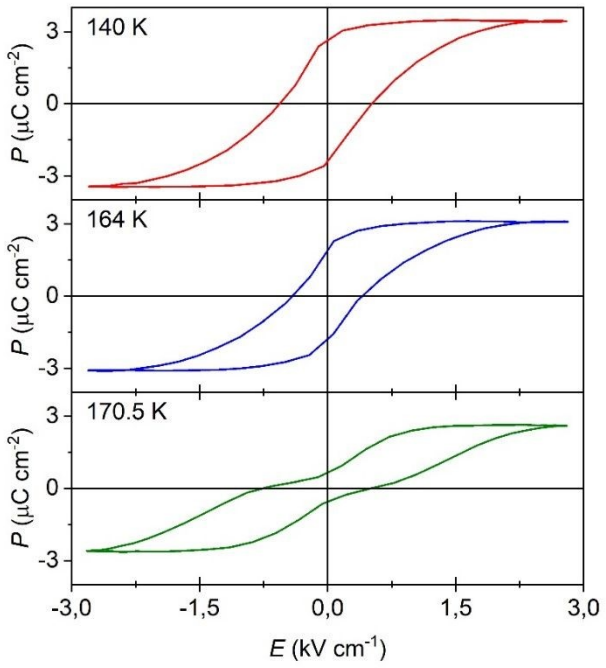

Figure 3. Selected polarization loops below (140 K and 164 K) and above the transition temperature T_1 at ν = 927 mHz.

The third transition between III (FE) and IV (AFE) commences at 180 K, and the last transition towards the paraelectric (PE) polymorph V occurs at 202 K. These transitions have been assigned following the literature.[5,6]

2.2. Electrocaloric effects in thiourea.

From now on, for the study of caloric effects we will focus on the first phase transition I-II due to its larger latent heat.

Below T_1 ~ 168 K, the polymorph I is ferroelectric and for 168 < T(*K*) < 175 the polymorph II is antiferroelectric, as observed by the polarization loops in Figure 3, which is in agreement with the literature.[5]

The FE phase exhibits a saturation polarization value of P_s ~ 3.5 μC cm^{-2} under the application of electric fields as small as 3 kV cm^{-1}. When undergoing the phase transition, thiourea exhibits a double polarization loop characteristic of antiferroelectric materials. Those loops exhibit a saturation polarization of P_s ~ 2.6 μC cm^{-2} when increasing the electric field up to 3 kV cm^{-1}.

These values of polarization agree with values obtained by the integration of the pyroelectric effect related to the FE-AFE transition with a P_s ~ 2.7 μC cm^{-2} (see Figure 4).

From the analysis of the polarization loops (Figure S1 of SI), we calculate the polarization change as a function of temperature for different applied electric fields (Figure 5).

Further analysis of these curves, help us to do a first indirect estimation of the isothermal entropy change, ΔS, using the Maxwell equation (1), which is a common method often used to evaluate electrocaloric effects in ferroelectric materials[13,32–34]:

$$\Delta S = -\frac{1}{\rho}\int_{E_1}^{E_2}\left(\frac{\partial P}{\partial T}\right)dE \quad (1);$$

where ρ is the density of the material.

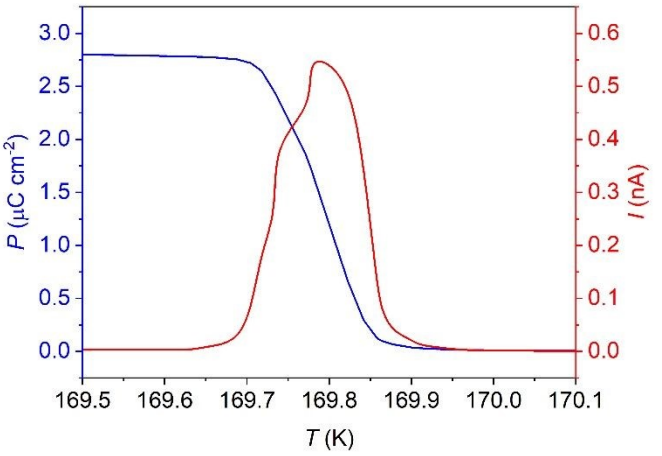

Figure 4. Temperature dependence of the spontaneous polarization (blue curve) by integrating the pyroelectric current (red curve).

As it can be observed in Figure 5, the isothermal entropy change increases up to 1.7 J K^{-1} kg^{-1} when applying an electric field as small as 1.5 kV cm^{-1}, giving a large electrocaloric strength of 1.13 J cm K^{-1} kg^{-1} kV^{-1}. This value is similar (and in some cases larger) than that shown by the best bulk electrocaloric materials reported up to date.[32,35–41]

According to the polarization *versus* temperature curves (Figure 5), that we have measured in the presence of different electric fields, the transition temperature shifts towards larger values when increasing the applied electric field with a dependency of dT_t/dE ~ 0.7 K cm kV^{-1}, which is in agreement with data obtained from the *E-T* phase diagram obtained by Futama in the I-II limiting region (dT_t/dE ~ 0.9 K cm kV^{-1}).[6] This very large displacement together with the very small thermal hysteresis observed in our VT-DSC studies, anticipate that the electrocaloric effects –here calculated as ΔS ~ 1.7 J K^{-1} kg^{-1} using the polarization curves– could be reversibly driven already under low applied electric fields.

For a deeper assessment of the electrocaloric effects, we have built VT-DSC curves using our experimental data, together with the *E-T* phase diagram reported in the literature.[6,7]

View Article Online
DOI: 10.1039/D5TA06231

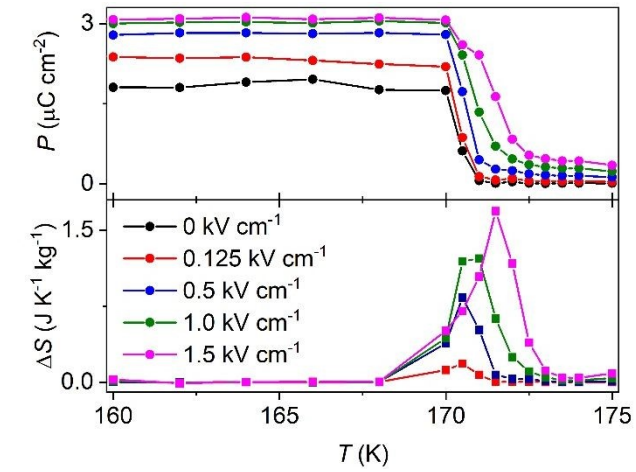

Figure 5. Polarization change (top) and isothermal entropy change (bottom) as a function of temperature at different applied external electric fields.

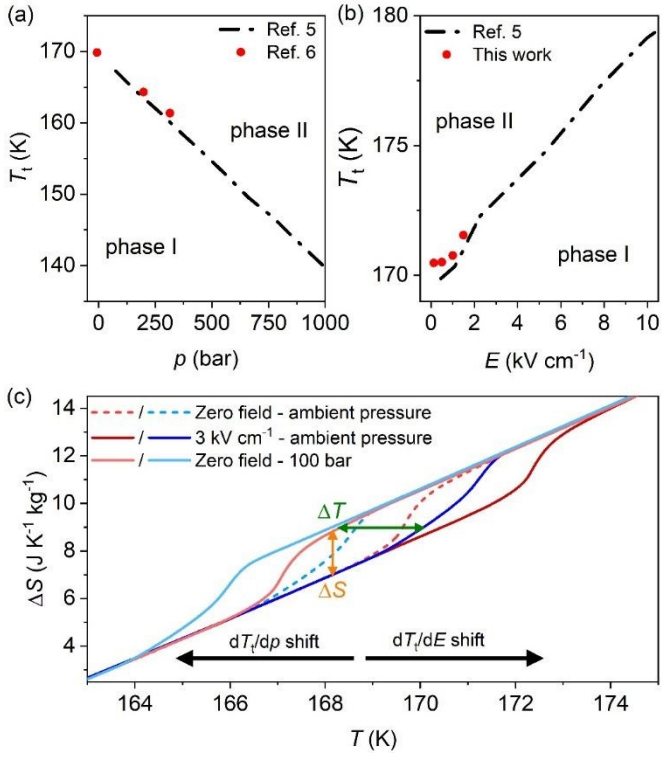

Figure 6. (a) Transition temperature dependence with pressure (dT_t/dp). (b) Transition temperature dependence with applied electric field (dT_t/dE). (c) Isothermal entropy change curves (ΔS) under different conditions: (i) at zero applied field and ambient pressure (dash lines), (ii) under the application of 3 kV cm^{-1} at ambient pressure, and (iii) under zero field at 100 bar. Note: heating curves in red, cooling curves in blue. Reversible values of ΔS and ΔT in orange and green arrows.

Furthermore, we have used the same strategy considering reported *p*-*T* phase diagrams[6] for evaluating the barocaloric behavior induced by applied pressure on thiourea.

Figure 6 shows the I-II transition temperature shift when applying pressure (panel a) and when applying electric field (panel b). According to these data, we found that thiourea displays an inverse barocaloric coefficient with values of dT_t/dp = -29.7 K kbar^{-1}, ranking among the largest barocaloric coefficients reported up to date.[42]

In the same line, Figure 6c shows the isothermal entropy change curves (ΔS) of the sample under different conditions: (i) at zero applied field and ambient pressure (dash lines), (ii) under the application of 3 kV cm^{-1} at ambient pressure, and (iii) under zero field at 100 bar (a pressure easily accessible by commercial compressors, especially in those of CO_2-based refrigeration systems).

These curves have been built considering the specific heat capacity C_p of thiourea[30] and our VT-DSC curves shifted according to the reported values of (dT_t/p) [6,7] and (dT_t/dE) [6]. This approach is a common practice in classic caloric studies, especially when very complex equipment would be required (i.e. calorimeter coupled to electric field and high pressure in this case).[43–45]

Under these assumptions, the isothermal entropy changes can be obtained using equation (2) as reported elsewhere [13]:

$$\Delta S = \int_{T_1}^{T_2} \frac{1}{T}\left(C_p(T,p_{atm}) + \frac{dQ}{dT}(T,i)\right)dT \quad (2).$$

where T_1 and T_2 indicate the arbitrary initial and final temperature, *i* represents the electric field (or pressure) for each $|dQ/dT|$ curve, and C_p is the heat capacity of the material for each temperature at atmospheric pressure (p_{atm}), which is considered independent from the applied pressure.

From these curves we can extract several important conclusions regarding the caloric effects of thiourea: (i) thiourea can present inverse barocaloric effects where the transition temperature shifts towards higher temperatures when increasing pressure; (ii) thiourea presents conventional electrocaloric effects where the transition temperature shifts towards higher temperatures when increasing the applied electric field, (iii) we can combined both applied electric field and pressure to increase the caloric effects of thiourea, obtaining pressure-assisted electrocaloric effects or multicaloric effects.

In that latter aspect, in Figure 6c it can be observed that when modulating the external conditions from zero field at 100 bar to 3 kV cm^{-1} at ambient pressure, the reversible caloric effects are ΔS~1.9 J K^{-1} kg^{-1} (orange arrow in Fig. 6c) and ΔT~1.8 K (green arrow in Fig. 6c). It should be noted that these values (particularly ΔS values) are in agreement with our previous calculations using the polarization curves under 1.5 kV cm^{-1}.

Even more remarkably, according to curves from Figure 6, the caloric effects can be already reversible under the application of a noticeable low electric field, only 3 kV cm^{-1}, and/or 100 bar, while most electrocaloric materials required electric field of 10 - 1200 kV cm^{-1} [20,21,32,35–41,46] and most barocaloric materials required pressures above 1000 bar.[42] The significant reduction of the required electric field and pressure open the door to designing safer devices with lower energy consumption and lower complexity.

View Article Online
DOI: 10.1039/D6TA00623J

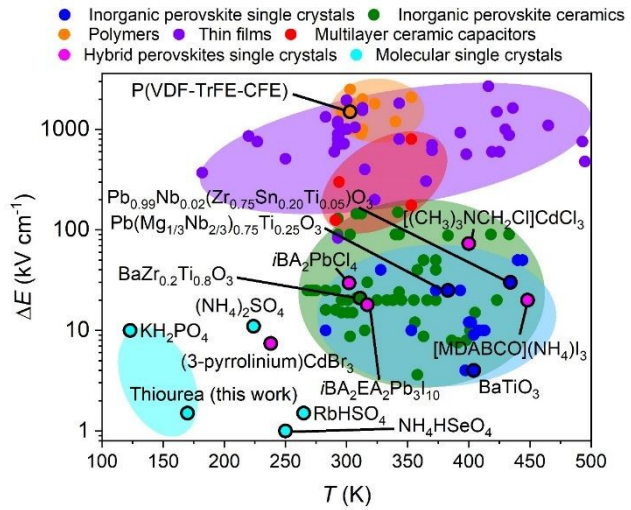

Figure 7. Comparison of different families of electrocaloric materials in terms of required electric field ΔE (kV cm^{-1}) for a given operating temperature T(K), where thiourea require a much lower electric field to display electrocaloric effects while being one of the very few examples to operate in the cryogenic region. Data compiled from references [20,21,32–41,46–50]. ***Note:*** Selected bulk electrocalorics from Table 1 are highlighted. *i*BA = isobutylammonium; EA = ethylammonium; DABCO = 1,4 Diazabicyclo[2.2.2]octane; P(VDF-TrFE-CFE) = poly(vinylidene fluoride-trifluoroethylene-chlorofluoroethylene)..

Table 1. Caloric parameters of the best bulk electrocaloric materials reported up to date. T_h is the transition temperature on heating, T_h - T_c is the thermal hysteresis, $|\Delta S|$ is the electrocaloric effect in terms of isothermal entropy change, $|\Delta E|$ is the externally applied electric field, $|\Delta S/\Delta E|$ is the electrocaloric strength in terms of entropy change, and $|dT_t/dE|$ is the electrocaloric tunability.

Material (bulk)	Sample type	T_h (K)	T_h-T_c (K)	$\lvert\Delta S\rvert$ (J K^{-1} kg^{-1})	$\lvert\Delta E\rvert$ (kV cm^{-1})	$\lvert\Delta S/\Delta E\rvert$ (J cm K^{-1} kg^{-1} kV^{-1})	$\lvert dT_t/dE\rvert$ (K cm kV^{-1})	Ref.
Thiourea	single crystal	170	1.0	1.7	1.5	1.13	0.7	This work
$(NH_4)_2SO_4$	single crystals	224	2.8	19.0	11.0	1.72	5 x 10^{-3}	48
$RbHSO_4$	single crystal	265	-	0.04	1.5	0.03	-	47
NH_4HSeO_4	single crystal	250	0.7	0.1	1.35	0.07	1.6	49
$iBA_2EA_2Pb_3I_{10}$	single crystal	~317	~6.0	33.3	18	1.85	-	34
iBA_2PbCl_4	single crystal	302	10	25.6	29.7	0.86	-	33
$[(CH_3)_3NCH_2Cl]CdCl_3$	single crystal	400	3.2	33.1	73	0.5	3.6 x 10^{-2}	50
$(3\text{-pyrrolinium})CdBr_3$	single crystal	238	2.7	1.2	7.4	0.16	-	32
$[MDABCO](NH_4)I_3$	single crystal	448	54.0	36.0	20.0	1.8	0.11	35
KH_2PO_4	single crystal	123	-	3.5	10	0.35	-	36
$BaTiO_3$	single crystal	404	2.0	2.1	4.0	0.5	0.33	37
$Pb(Mg_{1/3}Nb_{2/3})_{0.75}Ti_{0.25}O_3$	single crystal	383	-	-	25.0	-	-	38
$Pb_{0.99}Nb_{0.02}(Zr_{0.75}Sn_{0.20}Ti_{0.05})O_3$	single crystal	434	-	-	30.0	-	-	39
$BaZr_{0.2}Ti_{0.8}O_3$	ceramic	311	-	1.9	21.0	0.09	-	40
P(VDF-TrFE-CFE)	polymer	303	-	73.5	1500.0	0.05	-	41

Moreover, in order to further confirm the magnitude of the caloric effects, we also study the volume change across the phase transition (Figure S2 of SI) using single crystal X-ray diffraction, as further discussed in the following section. From this data, we can calculate the isothermal entropy change of the PI→PII phase transition related to the caloric effect using the Clausius-Clapeyron equation (3):

$$\Delta S = \frac{\Delta v}{\left(dT_t/dp\right)}$$

where Δv is the specific volume change across de transition and dT_t/dp is the barocaloric coefficient. Following this additional method, we confirm that the isothermal entropy change shows a value of ΔS ~ 1.5 J K-1 kg^{-1}, which is in agreement with the value calculated by Maxwell equation (ΔS ~ 1.7 J K-1 kg^{-1}) and

View Article Online
DOI: 10.1039/D6TA00623J

the value calculated from the constructed isothermal entropy change curves from Figure6 and equation 2 (ΔS ~ 1.9 J K-1 kg^{-1}). Moreover, the specific volume change as a function of temperature (Fig. S2 of SI) reveal that the transition temperature of the phase transition PI→PII takes place at T_t ~ 172 K, which is in fully agreement with the T_t values obtained by our variable-temperature DSC (Fig. 1) and polarization data (Fig. 5), as well as with the dielectric regions previously identified by Godschmith and White (Fig. 2).[5,6,8]

When analysing the caloric parameters, thiourea exhibits a large electrocaloric strength ($\Delta S/\Delta E$ = 1.13 J cm kg^{-1} kV^{-1}) and a electrocaloric tunability (dT_t/dE = 0.7 K cm kV^{-1}), which overpass those values of state-of-the-art *bulk* electrocaloric materials, such as the inorganic perovskite $BaTiO_3$ ($\Delta S/\Delta E$ = 0.5 J cm kg^{-1} kV^{-1}, dT_t/dE = 033 K cm kV^{-1})[37] and the metal-free perovskite MDABCO(NH_4)I_3 ($\Delta S/\Delta E$ =1.8 J cm kg^{-1} kV^{-1}, dT_t/dE = 0.11 K cm kV^{-1})[35], see Table 1.

Furthermore, thiourea exhibits its electrocaloric effects in the cryogenic temperature (~170 K) region where the only example is the also molecular compound KH_2PO_4, and while most reported electrocalorics operate near room temperature (250-500 K), see Figure 7.

2.3. Structural origin of the electrocaloric parameters

Most of the reported electrocaloric materials (including $BaTiO_3$ and MDABCO(NH_4)I_3) present an extended non-molecular structure where the atoms are bonded by strong chemical interactions (such as covalent and ionic bonds). Meanwhile, thiourea (similarly to KH_2PO_4) is a molecular compound where the bonding between the molecules is mainly based on weaker intermolecular interactions, namely hydrogen bonds. Additionally, the thiourea molecule is a low-molecular-weight polar species with a large electrical dipole of ~9 D[26] along the carbon-sulfur axis due to its planar conformation. Therefore, in comparison with large-molecular-weight species that are linked through stronger bonds, thiourea would require smaller electric fields to orient the electric dipoles and induce a phase transition, while allowing for the transition to occur at much lower temperatures.

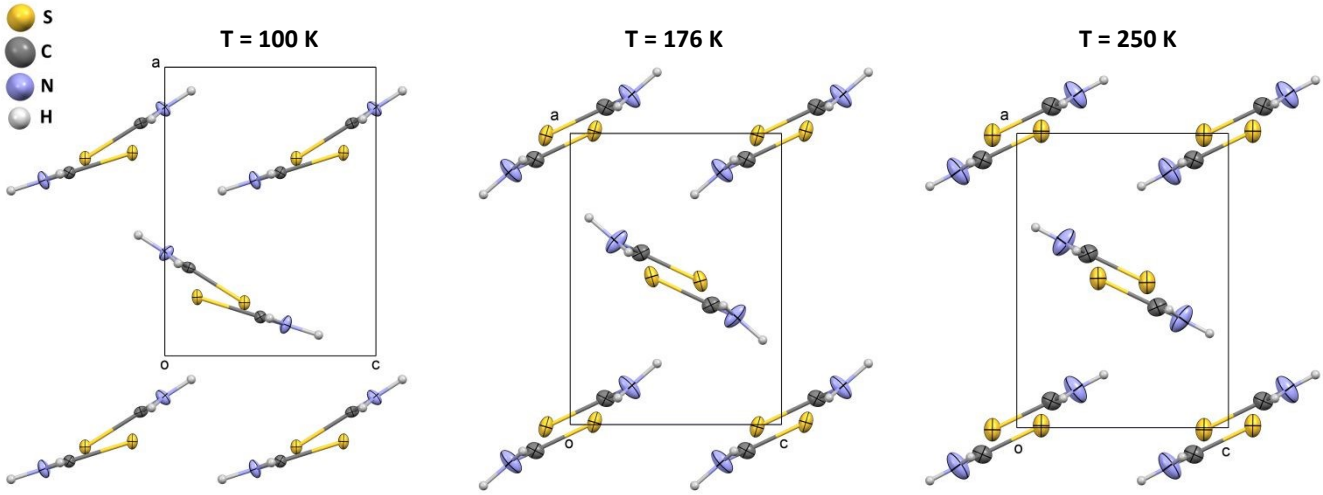

Figure 8. Crystal structures obtained by single-crystal x-ray diffraction at T=250 K, 176 K and 100 K.

In the literature it is possible to find different data sets for the crystal structures of thiourea that have been generated since the 30s up to date. As these data have been compiled by different authors using different temperature ranges, different crystals and different instruments that have advanced over the years, some contradictions in the data are almost inevitable.[8,51–56]

In this work, and for the first time, we have been able to determine the crystal structures of the low-temperature and high-temperature polymorphs I and V, as well as an averaged crystal structure for the modulated phases related to II, III and IV phase regions, using the same crystal sample and a "state of the art" single crystal diffractometer. In that manner, we have obtained a set of coherent and homogeneous results which can be the basis to look for structure- electrocaloric properties relationships.

According to our single crystal X-ray diffraction structure determination, at $T \leq 172$ K thiourea exhibits an orthorhombic phase I with space group $P2_1ma$ (non-centrosymmetric). Meanwhile, at $T \geq 202$ K phase V presents an orthorhombic symmetry and centrosymmetric space group *Pnma.* Additionally, phases II to IV (modulated phases) also exhibit an orthorhombic symmetry and centrosymmetric space group *Pnma* for the "average" structure refined using only the main reflections and not the satellite peaks. Raw collected and processed data considering the modulation and satellite peaks integration are also available in open access repository (see methods section).

The modulation vector describes the small structural changes that "breaks" the centrosymmetry allowing for the observed physical properties, like FE and AFE, otherwise forbidden. For the refined modulated phases, even if we have not taken the modulation peaks into account, we obtain good agreement

View Article Online DOI: 10.1039/D6TA00623J

factors between the proposed model and the experimental data.

In all the crystal structures studied from 100 to 250 K, thiourea molecules are packed forming chains along the *b*-axis, where neighboring molecules are alternatively rotated ~180º and slightly shifted out of the plane of the chains (see Figure 8 and S3 of SI). Thiourea molecules are linked by H-bonds from the nitrogen to the sulfur (N-H···S). We observe two different types of H-bonds: the first ones are shorter and occur within the same chains (intrachain H-bonds), and the second ones are longer and take place between neighboring chains (interchain H-bonds), see Figure S4 of SI.

Remarkably, we find that H-bonds play an important role in the observed phase transitions and dielectric response, as postulated in previous works[56,57] and further detailed below.

The high-temperature phase V exhibits an asymmetric unit which comprises half sulphur, half carbon, one nitrogen and two hydrogens with the first two atoms located over the crystallographic mirror plane. Here, thiourea molecules along the same chain are ordered in an antiparallel arrangement related by crystallographic symmetry centers where the dipoles cancel out.

In the whole temperature range studied, we observe that the intramolecular bonds lengths and angles of thiourea molecules are almost temperature independent. However, the disposition of the H-atoms and the relative orientations of thiourea molecules change with temperature.[56,57] We suggest that these distortions are provoked by changes in the H-bond strength as a function of temperature.

In this context, when the temperature lies between 168 K and 202 K (in the low-temperature phase and modulated phase regions), the H-atoms are located out the coplanar disposition. Meanwhile, when the temperature increases above 202 K, the H-atoms are displayed in a coplanar disposition.

It should be noted that the 2 crystallographically independent H-atoms exhibit slightly different out-of-plane displacement values (Table S2 of SI), but both are perfectly correlated.

As it can be seen in Figure S5 of SI, we find that these displacements increase at lower temperatures with a maximum value at T ~ 176 K, which coincides with a maximum of the real part of the relative permittivity related to FE phase III. Therefore, the displacement of the H-atoms, which is likely induced by the H-bonds strengthen at lower temperatures, seems to be responsible for the modulation of the crystal structures and for the dielectric transitions.

Below T ~ 176 K, the H-atom displacement decreases inducing a new distortion of the crystal structure related to the AFE to FE phase transition from polymorph II to I. As a consequence, in the low temperature phase I, two types of thiourea molecules appear which are no longer in a centrosymmetric arrangement, differently from phase V. In phase I, both types of thiourea molecules are slightly tilted breaking the anti-parallel arrangement and resulting in the appearance of a net polarization along the *a*-axis. From the crystallographic point of view, this tilting is described by the irreducible representation ($GM3^-$) of the parent space group *Pnma*, where the associated order parameter corresponds to the magnitudes of the tilting between neighbouring thiourea molecules.

In summary, we find that the H-bonds might be the driving force behind the structural and dielectric transitions in the thiourea crystals. The strength of this intermolecular interaction is strongly temperature dependent, which gives rise to the temperature-induced multiple transitions, including the AFE to FE transition responsible for the large electrocaloric effect. In addition, the relative weakness of these interactions allows an easy reorientation of the thiourea dipoles under an applied electric field, leading to the remarkably giant electrocaloric strength tunability found in this compound.

Conclusions

In this work, we report for the first time the electrocaloric effects of a classic organic compound that was one of the earliest and most intensively studied crystal structures and ferroelectric materials reported in the literature, thiourea.

Remarkably, this organic compound is one of the few examples of electrocaloric materials that can operate in the cryogenic temperature range, temperature regime that is attracting the interest of the scientific community working on electrocaloric materials and technologies. Furthermore, thiourea exhibits a significantly large electrocaloric strength ($\Delta S/\Delta E$ = 1.13 J cm kg^{-1} kV^{-1}) and electrocaloric tunability (dT_t/dE = 1.0 K cm kV^{-1}), which overpass the values found in state-of-the-art *bulk* electrocaloric materials and that is attributed to the significantly low operating electric field of only [1.5-3.0] kV cm^{-1}. Even more interestingly, we have identified that the ferroic transition responsible for the electrocaloric effect can be modulated with pressure, so thiourea can present enhanced pressure-assisted electrocaloric effects. Combining applied pressure and electric field, thiourea can present caloric effects of ΔS ~ 1.9 J K^{-1} kg^{-1} and ΔT ~ 1.8 K, turning this compound as a new example of the emerging category of multicaloric materials.

In addition, we have also deepened into the relationships between the structure and the electrocaloric effect looking for key aspects that allow us to clarify the origin of this outstanding behavior and give clues to design enhanced electrocaloric materials in the future. In this case, we find that the molecular nature of this compound with low molecular weight, an associated large electric dipole and weak chemical interactions between molecules, mainly H-bonds, are responsible for its large electrocaloric response and allow for the structural transitions to occur at lower temperatures than in most electrocaloric materials. These findings open the door to future studies on molecular electrocaloric materials with enhanced strengths and tunabilities.

Methods

Crystal preparation: Single crystals of thiourea (Figure S6 of SI) were grown using a method reported elsewhere.[5] For this purpose a saturated methanol solution of thiourea (Sigma Aldrich ≥99.0%) was maintained undisturbed to allow for evaporation in open air conditions. After a few weeks,

View Article Online
DOI: 10.1039/D5TA06231

transparent millimeter-sized and hexagonal-plate shaped single crystals were obtained.

Single crystal x-ray diffraction: Single-crystal X-ray diffraction experiments were carried out at different temperatures starting below to above all the phase transitions. For that purpose, 17 single-crystal diffraction data sets of one crystal were collected at different temperatures between 100 and 250 K in a Bruker D8 VENTURE Kappa X-ray diffractometer equipped with a PHOTON III detector and using monochromatic MoKα radiation (λ=0.71073 Å).

A suitable crystal was chosen and mounted on a MiTeGen MicroMount™ using Paratone® N (Hampton Research). The temperature of the crystal was changed at 200 K / hour rate blowing the sample with a stream of nitrogen gas from an Oxford Cryosystem 800 Plus cooler. The data integration and reduction were performed using the APEX3 v2019.1-0[58] software suite. The integrations of the reflections were performed with SAINT 8.38A and the intensities collected were corrected for Lorentz, polarization effects and for absorption by semi-empirical methods based on symmetry-equivalent data using SADABS 2016/2 of the APEX3 suite software. The structures were solved by the dual-space algorithm implemented in SHELXT2018/2[59] program and were refined by least squares method on SHELXL2018/3.[60]

Detailed experimental crystallographic data for thiourea at T = 100, 130, 150, 160, 165, 170, 172, 174, 176, 178, 180, 185, 190, 200, 202, 210, and 250 K are included in Tables S1 of SI. CCDC 2039156-2039172 contains the supplementary crystallographic data for this paper. These data can be obtained free of charge from The Cambridge Crystallographic Data Centre via www.ccdc.cam.ac.uk/structures. Full raw diffraction datasets for the 17 measured temperatures are hosted and completely available on Zenodo (https://zenodo.org/communities/thiourea) to ensure reproducibility and long-term data preservation.

Dielectric and ferroelectric properties: The real (ε') and imaginary (ε'') parts of the dielectric permittivity were measured using a Precision LCR Meter (HP 4284 A) in the frequency range 10^2-10^6 Hz and using a voltage of 0.1 V. For that purpose, we deposited gold electrodes (area ~0.14 mm^2) on a crystal oriented along the polar axis (length ~2 mm). The temperature was controlled using a He closed cycle cryogenic system (Displex ADP-Cryostat HC-2), equipped with a digital temperature controller (IEE-488 Status). The temperature range measured varied from 10 K to 300 K with a rate of 1 K min^{-1}. In addition, we registered the Cole-Cole diagrams between 160 K and 170 K.

The ferroelectric hysteresis loops (P-E) were traced by a modified Sawyer-Tower[17] circuit using a sinusoidal signal at a frequency of 927 mHz.

Pyroelectric properties:

The pyroelectric behavior was examined with a direct method, in which the charge released with a given incremental temperature change as a function of temperature was measured with a Keithley 617 electrometer. For this purpose, gold electrodes (area ~0.14 mm^2) were sputtered on opposite sides of a single crystal (length ~2 mm). The sample was first cooled in an electric field (50 V) from 190 K to 140 K (rate 1 K min^{-1}); then, the electric field was removed and the $I(T)$ curve was recorded using a temperature sweep of 1 K min^{-1} heating and cooling rate. Before heating from 140 to 190 K and cooling from 190 K to 140 K a time dependence of electric charge was recorded for 1800 s to ensure stability. The polarization was calculated following equation 4 as reported elsewhere[61]:

$$P = \frac{1}{r\,A}\int_{T_1}^{T_2} I\,dT \quad (4)$$

where r is the heating/cooling rate, A is the electrode area, and I is the pyroelectric current.

Differential scanning calorimetry:

Differential scanning calorimetry was carried out in an Setaram Setline DSC in the range of 130 – 180 K with a heating/cooling ramp of 1 K min^{-1}, using ~4 mg of sample. For indirect assessment of electrocaloric and barocaloric measurements, the curves were displaced following the dependence of the transition temperature with the electric field and with the pressure as reported in the literature.[6,7]

Acknowledgements

The authors thank financial support from grant PID2021-122532OB-I00 funded by MCIU/AEI/10.13039/501100011033 and ERDF/EU, and the projects ED431C 2022/39 and ED431F 2023/33 funded by Xunta de Galicia. This publication is part of the grant RYC2021-033040-I, funded by MCIU/AEI/10.13039/501100011033 and from European Union «NextGenerationEU»/PRTR». J. M. B.-G. is grateful for the support received by UDC-Inditex InTalent Programme.

Author contributions

The manuscript was written through contributions of all authors. All authors have given approval to the final version of the manuscript. ‡These authors contributed equally.

Data availability

The data supporting this article have been included as part of the Electronic Supplementary Information.

The raw X-ray diffraction data (including integrated intensities and frame images) for all 17 temperatures reported in this study are openly available in Zenodo at https://zenodo.org/communities/thiourea. Each dataset is associated with a unique DOI, which is also linked to the corresponding CCDC deposition numbers (2039156-2039172). Additional data will be available from authors upon reasonably request.

Competing interests

The authors declare no competing interests.

References:

1 F. Wöhler, *Ann. Phys.*, 1828, **88**, 253–256.
2 M. Nencki, *Ber. Dtsch. Chem. Ges.*, 1873, **6**, 598–600.
3 R. W. G. Wyckoff and R. B. Corey, *Zeitschrift für Krist.* -

Cryst. Mater., 1932, **81**, 386.
4 A. L. Solomon, *Phys. Rev.*, 1956, **104**, 1191.
5 G. J. Goldsmith and J. G. White, *J. Chem. Phys.*, 1959, **31**, 1175–1187.
6 H. Futama, *J. Phys. Soc. Japan*, 1962, **17**, 434–441.
7 K. Gesi, *J. Phys. Soc. Japan*, 1969, **26**, 107–112.
8 Y. Shiozaki, *Ferroelectrics*, 1971, **2**, 245–260.
9 D. R. McKenzie and J. S. Dryden, *J. Phys. C Solid State Phys.*, 1973, **6**, 767–773.
10 A. H. Moudden, F. Denoyer, M. Lambert and W. Fitzgerald, *Solid State Commun.*, 1979, **32**, 933–936.
11 A. H. Moudden, D. E. Moncton and J. D. Axe, *Phys. Rev. Lett.*, 1983, **51**, 2390–2393.
12 C. P. Menon and J. Philip, *Ferroelectrics*, 2003, **287**, 63–70.
13 X. Moya, S. Kar-Narayan and N. D. Mathur, *Nat. Mater.*, 2014, **13**, 439–450.
14 E. Defay, R. Faye, G. Despesse, H. Strozyk, D. Sette, S. Crossley, X. Moya and N. D. Mathur, *Nat. Commun.*, 2018, **9**, 1827.
15 B. Nair, T. Usui, S. Crossley, S. Kurdi, G. G. Guzmán-Verri, X. Moya, S. Hirose and N. D. Mathur, *Nature*, 2019, **575**, 468–472.
16 A. Bergen, R. Andersen, M. Bauer, H. Boy, M. ter Brake, P. Brutsaert, C. Bührer, M. Dhallé, J. Hansen, H. ten Kate, J. Kellers, J. Krause, E. Krooshoop, C. Kruse, H. Kylling, M. Pilas, H. Pütz, A. Rebsdorf, M. Reckhard, E. Seitz, H. Springer, X. Song, N. Tzabar, S. Wessel, J. Wiezoreck, T. Winkler and K. Yagotyntsev, *Supercond. Sci. Technol.*, 2019, **32**, 125006.
17 W. Chen, M. DiPirro, I. McKinley, C. Cho and H. Tseng, *Cryogenics*, 2024, **141**, 103877.
18 A. Rai and S. A. Tassou, *Energy Convers. Manag.*, 2017, **150**, 914–923.
19 K. Klinar, J. Y. Law, V. Franco, X. Moya and A. Kitanovski, *Adv. Energy Mater.*, 2024, **14**, 2401739.
20 A. Barman, S. Kar-Narayan and D. Mukherjee, *Adv. Mater. Interfaces*, 2019, **6**, 1–31.
21 J. Shi, D. Han, Z. Li, L. Yang, S. G. Lu, Z. Zhong, J. Chen, Q. M. Zhang and X. Qian, *Joule*, 2019, **3**, 1200–1225.
22 X. Chen, W. Zhu and Q. M. Zhang, *iEnergy*, 2023, **2**, 100–108.
23 J. Mira, J. Rivas, L. E. Hueso, F. Rivadulla and M. A. López-Quintela, *J. Appl. Phys.*, 2002, **91**, 8903–8905.
24 J. Mira, F. Rivadulla, J. Rivas, A. Fondado, T. Guidi, R. Caciuffo, F. Carsughi, P. G. Radaelli and J. B. Goodenough, *Phys. Rev. Lett.*, 2003, **90**, 189901.
25 J. M. Bermúdez-García, M. Sánchez-Andújar, S. Castro-García, J. López-Beceiro, R. Artiaga and M. A. Señarís-Rodríguez, *Nat. Commun.*, 2017, **8**, 15715.
26 M. Gelpi, J. García-Ben, S. Rodríguez-Hermida, J. López-Beceiro, R. Artiaga, Á. Baaliña, M. Romero-Gómez, J. Romero-Gómez, S. Zaragoza, J. Salgado-Beceiro, J. Walker, C. J. McMonagle, S. Castro-García, M. Sánchez-Andújar, M. A. Señarís-Rodíguez and J. M. Bermúdez-García, *Adv. Mater.*, 2024, **36**, 2310499.
27 L. Abate, M. Jozwiak and G. Della Gatta, *Thermochim. Acta*, 1997, **303**, 63–68.
28 G. Della Gatta, M. Jóźwiak, B. Brunetti and L. Abate, *J. Chem. Thermodyn.*, 2000, **32**, 979–997.
29 S. Wang, Q. Gao and J. Wang, *J. Phys. Chem. B*, 2005, **109**, 17281–17289.
30 J. M. Igartua, A. LÓpez-Echarri, T. Breczewsk and I. Ruiz-Larrea, *Phase Transitions*, 1993, **46**, 47–55.
31 T. Hess, L. M. Maier, N. Bachmann, P. Corhan, O. Schäfer-Welsen, J. Wöllenstein and K. Bartholomé, *J. Appl. Phys.*, 2020, **127**, 075103.
32 P. F. Li, W. Q. Liao, Y. Y. Tang, H. Y. Ye, Y. Zhang and R. G. Xiong, *J. Am. Chem. Soc.*, 2017, **139**, 8752–8757.
33 X. Liu, Z. Wu, T. Guan, H. Jiang, P. Long, X. Li, C. Ji, S. Chen, Z. Sun and J. Luo, *Nat. Commun.*, 2021, **12**, 1–7.
34 S. Han, J. Bie, W. Fa, S. Chen, L. Tang, W. Guo, H. Xu, Y. Ma, Y. Liu, X. Liu, Z. Sun and J. Luo, *J. Am. Chem. Soc.*, 2024, **146**, 8298–8307.
35 J. J. Wang, D. Fortino, B. Wang, X. Zhao and L. Q. Chen, *Adv. Mater.*, 2020, **32**, 1–6.
36 H. B. von Bern, *Helv. Phys. Acta*.
37 X. Moya, E. Stern-Taulats, S. Crossley, D. González-Alonso, S. Kar-Narayan, A. Planes, L. Mañosa and N. D. Mathur, *Adv. Mater.*, 2013, **25**, 1360–1365.
38 G. Sebald, L. Seveyrat, D. Guyomar, L. Lebrun, B. Guiffard and S. Pruvost, *J. Appl. Phys.*, 2006, **100**, 124112.
39 B. A. Tuttle and D. A. Payne, *Ferroelectrics*, 1981, **37**, 603–606.
40 X. S. Qian, H. J. Ye, Y. T. Zhang, H. Gu, X. Li, C. A. Randall and Q. M. Zhang, *Adv. Funct. Mater.*, 2014, **24**, 1300–1305.
41 X. Li, X. Qian, S. G. Lu, J. Cheng, Z. Fang and Q. M. Zhang, *Appl. Phys. Lett.*, 2011, **99**, 052907.
42 Y. Sun, S. An, Y. Gao, Z. Yu, X. Yuan, Z. Ma, K. Shi, F. Hu and C. Wang, *J. Mater. Chem. A*, 2025, 6152–6175.
43 M. V. Gorev, E. A. Mikhaleva, I. N. Flerov and E. V. Bogdanov, *J. Alloys Compd.*, 2019, **806**, 1047–1051.
44 M. V. Gorev, E. V. Bogdanov and I. N. Flerov, *Scr. Mater.*, 2017, **139**, 53–57.
45 M. V. Gorev, E. V. Bogdanov and I. N. Flerov, *J. Phys. D. Appl. Phys.*, 2017, **50**, 384002.
46 N. Saadatkhah, A. Carillo Garcia, S. Ackermann, P. Leclerc, M. Latifi, S. Samih, G. S. Patience and J. Chaouki, *Can. J. Chem. Eng.*, 2020, **98**, 34–43.
47 E. A. Mikhaleva, I. N. Flerov, V. S. Bondarev, M. V. Gorev, A. D. Vasiliev and T. N. Davydova, *Ferroelectrics*, 2012, **430**, 78–83.
48 V. S. Bondarev, E. A. Mikhaleva, M. V. Gorev and I. N. Flerov, *J. Alloys Compd.*, 2021, **892**, 162130.
49 V. S. Bondarev, E. A. Mikhaleva, M. V. Gorev and I. N. Flerov, *Solid State Commun.*, 2025, **395**, 115747.
50 Y. Lin, C. Chai, Z. Liu, J. Wang, S. Jin, Y. Yang, Y. Gao, M. Hao, X. Li, Y. Hou, X. Ma, B. Wang, Z. Wang, Y. Kan, J. Zheng, Y. Bai, Y. Chen, J. Sun, T. Zhao, J. Y. Law, V. Franco, F. Hu and B. Shen, *Nat. Commun.*, 2025, **16**, 4009.
51 D. R. McKenzie, *J. Phys. C Solid State Phys.*, 1975, **8**, 1607–1619.
52 A. Yamamoto, *Phys. Rev. B*, 1980, **22**, 373–379.
53 S. Tanisaki, H. Mashiyama and K. Hasebe, *Acta Crystallogr. Sect. B*, 1988, **44**, 441–445.

View Article Online
DOI: 10.1039/D6TA00623J

54 Y. Gao, M. Gajhede, P. Mallinson, V. Petricek and P. Coppens, *Phys. Rev. B*, 1988, **37**, 1825–1831.
55 Y. Gao and P. Coppens, *Acta Crystallogr. Sect. B*, 1989, **45**, 298–303.
56 I. Takahashi, A. Onodera and Y. Shiozaki, *Acta Crystallogr. Sect. B*, 1990, **46**, 661–664.
57 V. Petricek, P. Coppens and P. Becker, *Acta Crystallogr. Sect. A*, 1985, **41**, 478–483.
58 Bruker. *APEX3*, versión 2019.1-0; Bruker AXS Inc.: Madison, Wisconsin, USA, 2019.
59 G. M. Sheldrick, *Acta Crystallogr. Sect. A Found. Crystallogr.*, 2015, **71**, 3–8.
60 G. M. Sheldrick, *Acta Crystallogr. C Struct. Chem.*, 2015, **71**, 3–8.
61 H. Kaddoussi, A. Lahmar, Y. Gagou, B. Asbani, G. Cordoyiannis, B. Allouche, H. Khemakhem, Z. Kutnjak and M. El Marssi, 2016, **667**, 198–203.

View Article Online
DOI: 10.1039/D6TA00623J

Data availability statement (DAS):

The data supporting this article have been included as part of the Electronic Supplementary Information.

The raw X-ray diffraction data (including integrated intensities and frame images) for all 17 temperatures reported in this study are openly available in Zenodo at https://zenodo.org/communities/thiourea. Each dataset is associated with a unique DOI, which is also linked to the corresponding CCDC deposition numbers (2039156-2039172).

Additional data will be available from authors upon reasonably request.